Structural properties and phase transition of hole-orbital-ordered $(C_2H_5NH_3)_2CuCl_4$ studied by resonant and non-resonant x-ray scatterings under high pressure

Kenji Ohwada,* Kenji Ishii, Toshiya Inami, Youichi Murakami,† and Takahisa Shobu
Synchrotron Radiation Research Center (SPring-8), Japan Atomic Energy Research Institute, 1-1-1 Kouto, Mikazuki, Sayo, Hyogo 679-5148, Japan

Hiroyuki Ohsumi, Naoshi Ikeda, and Yasuo Ohishi
Japan Synchrotron Radiation Research Institute (SPring-8), 1-1-1 Kouto, Mikazuki, Sayo, Hyogo 679-5198, Japan

(Received 9 March 2005; revised manuscript received 31 May 2005; published 22 July 2005)

The effects of hydrostatic pressure on a structure and the corresponding resonant x-ray scattering (RXS) spectrum have been investigated for the hole-orbital-ordered compound $(C_2H_5NH_3)_2CuCl_4$. We have found a structural phase transition at $P_c \sim 4$ GPa, as suggested by the Raman scattering measurement, by observing a peak splitting resulting from an orthorhombic-to-monoclinic symmetry breaking. The reduction of the Jahn-Teller distortion (JTD) toward P_c is also ascertained by structural analyses. The gradual change in the color of the crystal is also observed in connection with the structural change near P_c. The red-colored transparency of the crystal indicates that the system is still insulative above P_c. The observed RXS and fluorescence spectrum at ambient pressure were precisely analyzed. We experimentally confirmed that the RXS intensity comes from the polarization of the density of states of p_x and p_y symmetries, which is mainly dominated not by the on-site $3d$-$4p$ Coulomb interaction but by the JTD of the $CuCl_6$ octahedron. charged Cl ions neighboring the Cu site. It is also expected that the RXS intensity is proportional to JTD; however, our RXS study under a high pressure shows no striking change as JTD is suppressed by the application of pressure. On the other hand, the RXS intensity becomes zero above P_c. The results indicate that the local environment of the Cu^{2+} ion markedly changes. Two possible structures of EA_2CuCl_4 above P_c are proposed.

DOI: 10.1103/PhysRevB.72.014123 PACS number(s): 62.50.+p, 71.27.+a, 61.10.Nz

I. INTRODUCTION

It has been recognized that the interplay of the lattice and the electronic degrees of freedom determines the electronic and magnetic properties of transition-metal compounds. In the case of the present subject material, the layer-perovskite compounds alkyl-ammonium tetrachloro-cuprates $(C_nH_{2n+1}NH_3)_2CuCl_4$ $(n=1,2,3\ldots)$, intraplane ferromagnetic (FM) interaction is associated with antiferro (AF) -hole-orbital ordering on the Cu^{2+} ions with the AF-distortive (AFD) arrangement of the elongated octahedra in the *ab* plane.

The series of compounds $(C_nH_{2n+1}NH_3)_2CuCl_4$ $(n=1,2,3\ldots)$ crystallizes in a layered perovskite structure consisting of nearly isolated layers of corner-sharing $CuCl_6$ octahedra sandwiched by alkyl-ammonium cations $(C_nH_{2n+1}NH_3)^+$, abbreviated MA (methyl-ammonium) for $n=1$ and EA (ethyl-ammonium) for $n=2$. Figure 1(a) shows a schematic drawing of the reported crystal structure of EA_2CuCl_4 at room temperature (RT) and ambient pressure (AP). The cavities between the octahedra are occupied by the NH_3 group of the alkyl-ammonium cations strongly coupled with the apical chlorine of a $CuCl_6$ octahedron through the N—H···Cl hydrogen bond as represented by the dotted lines in Fig. 1(a). Adjacent layers are stacked upon one another through van der Waals force between the terminal methyl groups. The crystal structure of EA_2CuCl_4 at RT and AP is orthorhombic ($a=7.47$ Å, $b=7.35$ Å, and $c=21.18$ Å) with the space group D_{2h}^{15}-P*bca*,[1,2] where all Cu sites are crystallographically equivalent.

Figure 1(b) shows a top view of the structure of EA_2CuCl_4, where the $CuCl_6$ octahedra are color coded for the discussions in Sec. III D. The $CuCl_6$ octahedra are strongly deformed due to the cooperative Jahn-Teller (JT) effects [called JT distortion (JTD)] and are in AFD arrangement. The elongated axis lies in the *ab* plane and is orthogonal to those in adjacent $CuCl_6$ octahedra, where the shorter and longer Cu—Cl distances are 2.28 Å ($Cu—Cl_{short}$) and 2.98 Å ($Cu—Cl_{long}$), respectively.[1] The JT effect lifts the degeneracy of the e_g orbital in the $t_{2g}^6 e_g^3$ electron configuration of the Cu^{2+} ($3d^9$) ions, and then the hole in the $3d$ shell occupies the d-orbit perpendicular to the local axis of the elongation resulting in the AF-hole-orbital ordering $-d_{x^2-z^2}-d_{y^2-z^2}-d_{x^2-z^2}-d_{y^2-z^2}\ldots$ with the AFD arrangement of the elongated octahedra in the *ab* plane. The intraplane FM superexchange interaction $J/k_B=18.6$ K between nearest-neighbor spins on the Cu sites is caused by the AF-hole-orbital ordering in EA_2CuCl_4. Due to the very weak interlayer antiferromagnetic (AFM) interaction $J'/J \simeq -8\times10^{-4}$, EA_2CuCl_4 transforms into the three-dimensional antiferromagnetic ordered states below $T_N=10.2$ K, where the spins are collinearly aligned in each layer along the *a* axis. Such an AF-hole-orbital ordering and associating intraplane ferromagnetism are directly observed in the prototypical AF-hole-orbital-ordered compound K_2CuF_4 by polarized neutron scattering.[3] The difference between EA_2CuCl_4 and K_2CuF_4 is the spin arrangement along the *c* axis, the former is AFM and the latter is FM, while both intralayer spin arrangements are FM.

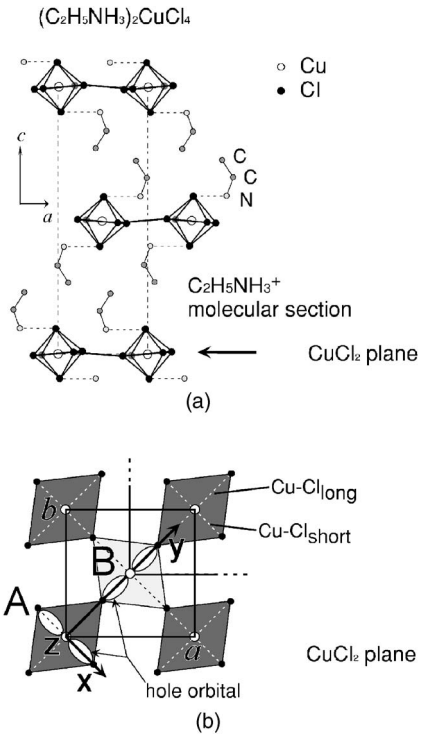

FIG. 1. (a) Schematic drawing of structure of EA_2CuCl_4 at room temperature and ambient pressure. The space group belongs to orthorhombic, D_{2h}^{15}-$Pbca^2$, and the lattice constants are a=7.47 Å, b=7.35 Å, and c=21.18 Å (Refs. 1 and 2). All Cu sites are crystallographically equivalent. Hydrogen, which is not shown in this figure, connects the apical chlorine with nitrogen. The N—H…Cl hydrogen bond is denoted by a dotted line. (b) The two sublattices in the ab plane of EA_2CuCl_4 marked A (dark-colored octahedron) and B (bright-colored octahedron), and two local axes (x and y) are shown. Both of sublattices and axes are defined to explain the RXS results in Sec. III D.

An application of high pressure is a way to control such a JT distortion, which strongly interacts with the electronic degrees of freedom, and in an extreme case, induces a structural phase transition and significantly changes the electronic and magnetic properties. Recently, quite interesting phenomena have been observed in EA_2CuCl_4 under high pressures. The application of pressure was found to suppress the JT effect by Raman scattering.[4] The reduction of the JT effect is proven by the deactivation of the Cu—Cl stretching mode (A_g) at approximately 180 cm^{-1} (A mode), which is Raman active and JTD sensitive. The charge-transfer (CT) type optical energy gap is also largely reduced by ~0.4 eV with the suppression of JTD. The intensity of the A mode decreases as the pressure increases and eventually vanishes above $P_c \sim 4$ GPa. It is inferred that the JT effect associated with the hole-orbital ordering is suppressed at 4 GPa and transforms into another phase, where the system is still insulative with a non-JTD arrangement or with another type of JTD arrangement. Similar phenomena have also been observed in $LaMnO_3$.[5] Raman scattering and x-ray structural analysis clarified that JTD and the corresponding orbital order in $LaMnO_3$ are completely suppressed at 18 GPa. However, the system remains insulating up to ~32 GPa, where it undergoes an insulator-to-metal transition. In this case, the insulating state at approximately 18 ~ 32 GPa is supposed to be a Mott-Hubbard insulator without JTD rather than a JTD-induced insulator.

The system with such an AFD octahedron arrangement associated with the AF-orbital-ordering gives a resonant x-ray scattering (RXS) intensity at symmetrically prohibited reflection spots. In 1998, Murakami *et al.* successfully observed the RXS intensity at the forbidden reflection spot 300 just at the Mn K-absorption-edge on the typical AF-orbital-ordered system $LaMnO_3$.[6] After that discovery, RXS has been observed in many perovskite systems such as the FM cuprate $KCuF_3$.[7] The recent first-principle calculation on $LaMnO_3$ and $KCuF_3$ has demonstrated that the RXS intensity is given by JTD with the modification of the 4p states of Mn (Cu) via the oxygen (fluorine) potential on the neighboring sites.[8–12] These calculations also show that the RXS intensity smoothly depends on the strength of JTD[8–12] That is to say, the RXS intensity is thought to be a good indicator of the evolution of the local distortion in such a JT-distorted system. Turning our attention to EA_2CuCl_4, it is interesting how the RXS intensity changes below and above P_c with the suppression of the JT effect associated with the hole-orbital ordering. To begin with, is there structural phase transition at 4 GPa as predicted by the Raman scattering?[4] In this study, we have investigated the phase transition at 4 GPa and studied the effects of hydrostatic pressure on the lattice and the electronic structure in EA_2CuCl_4 by making use of the structural analysis, RXS, the x-ray absorption spectroscopy (XAS), and so on. We have experimentally confirmed that the RXS intensity observed at AP comes from the polarization of the density of states (DOS) of p_x and p_y symmetries and have particularly noted how the RXS intensity changes with pressure, i.e., as the JT effect associated with the suppression of the AF-hole-orbital ordering.

The present paper is organized as follows: experimental details are given in Sec. II. In Secs. III A–III C, we will present a direct observation of the orthorhombic-to-monoclinic phase transition at P_c and the tendency for the reduction of JTD below P_c. Next, we will present the results and the precise analyses of the RXS study of EA_2CuCl_4 at AP in Sec. III D. In Sec. III E, we will describe the pressure dependence of the RXS study. Finally, we will be able to mention the characteristic origin and the mechanism of the RXS spectrum from the present EA_2CuCl_4 system. Discussions are given in each section.

II. EXPERIMENTAL

Crystals of EA_2CuCl_4 were grown by a slow evaporation method from an aqueous solution containing stoichiometric quantities of $C_2H_5NH_2 \cdot HCl$ and $CuCl_2 \cdot H_2O$. The obtained crystals whose color was transparent yellow were thin and tender plates. We chose single-domain crystals at all times.

For all high-pressure experiments, a conventional diamond anvil cell (DAC) was used. Pressure was generated in a DAC using a 1:1 mixture of n-pentane:i-pentane pressure transmitting media, which guarantee a hydrostatic pressure of up to 6 GPa. For pressure determination, two pressure

markers were chosen to suit the following experiments, i.e., ruby fluorescence[13] for powder diffraction experiments and the lattice constant of NaCl[14] for single-crystal diffraction experiments. All high-pressure experiments were performed while increasing pressure.

The single crystal of EA_2CuCl_4 with a typical size of $(100\times100\times20)$ μm^3 $(a\times b\times c)$ was carefully prepared so as not to induce a strain on the sample and was mounted on the DAC. Overall, the behavior of the crystal lattice of EA_2CuCl_4 under pressure was studied by conventional scintillation-counter-methods using a MoKα radiation source monochromatized by PG(002) reflection at an x-ray power of 55 kV $\times$ 280 mA.

The trend of the pressure-induced structural change of EA_2CuCl_4 was investigated using synchrotron powder x-ray diffraction techniques at BL10XU of SPring-8. The polycrystalline sample of EA_2CuCl_4 mounted on the DAC was prepared by precipitation method in order to obtain a fine powder, which gives a homogeneous intensity distribution in a Debye-Scherrer ring. Wavelength was tuned to 0.4957 Å with a Si(111) double-crystal monochromator. A flat imaging plate (IP) was used as a detector. Debye-Scherrer rings recorded on the imaging plate were converted to conventional one-dimensional intensity vs 2θ (deg.) data.

The RXS and XAS measurements were performed at the synchrotron radiation beam lines BL02B1 (SPring-8) and BL-4C (Photon Factory). The incident x-ray was monochromatized using a Si(111) double-crystal monochromator and was in the σ polarization. The x-ray energy near the Cu K-absorption-edge (8.98 keV) was used, which was calibrated by the absorption edge of a Cu metal foil. A large single crystal with a typical size of $(5\times10\times0.1)$ mm^3 $(a\times b\times c)$ can be used for AP measurements. A solid-state detector (SSD) was also used to remove the contribution of higher harmonic x-rays. Polarization analysis was not applied in the present study. All RXS measurements were performed very carefully so as not to damage the sample by irradiation (refer to Appendix A).

III. EXPERIMENTAL RESULTS AND DISCUSSION

A. Structural phase transition at 4 GPa

First of all, we have studied the phase transition of EA_2CuCl_4 at $P_c\sim4$ GPa, which was predicted by Raman scattering.[4] By measuring some independent Bragg reflections, we have found that the peaks split along the c axis at P_c except for $h0l$ $(h,l=\text{integer})$ reflections. Figure 2 shows the pressure dependence of the 02L scan. The 020 Bragg peak starts to split into two peaks along the c^* direction above P_c. After the phase transition, the angle α between b and c, rapidly increases as shown in Fig. 3(c). This is direct evidence of the orthorhombic-to-monoclinic structural phase transition. As seen from the data taken at 4.25 GPa, the 020 peak and split twin peaks coexist, which means the phase transition is of the first order. Since the transition is *weakly* of the first order, which will be discussed later, the possible space group of the high-pressure phase is $C_{2h}^5-P2_1/a^2$ with the unique axis b (cell choice 3) achieved by the cell transformations $a\rightarrow b'$, $b\rightarrow a'$, $b+c\rightarrow2c'$, and $\alpha\rightarrow\beta'$, which is a subgroup of $Pbca$. The space group is the same as that of $(CH_3NH_3)_2CuCl_4$ (MA_2CuCl_4).[15]

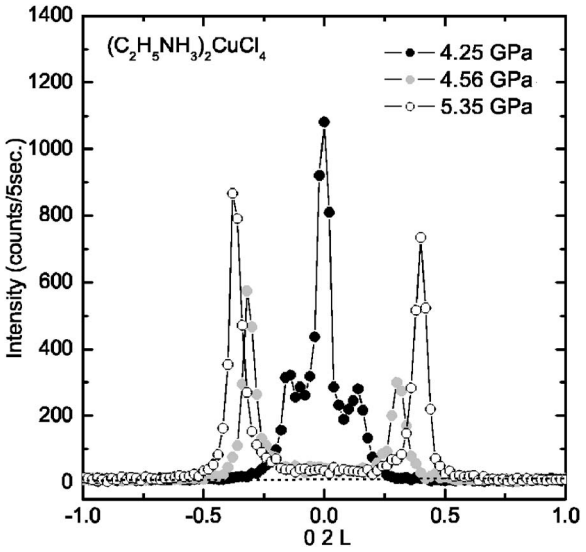

FIG. 2. Pressure dependence of 02L scan. 020 Bragg peak splits into two peaks along the c^* direction (L) above $P_c\sim4$ GPa. This is direct evidence of the orthorhombic-to-monoclinic structural phase transition.

Since the irradiation-damaged crystal of EA_2CuCl_4 shows no clear phase transition at P_c, the phase transition at P_c is a good indicator of the degree of irradiation damage. Details are mentioned in Appendix A.

B. Pressure dependence of lattice constants and piezochromism

Figures 3(a)–3(c) show the pressure dependence of the lattice parameters a, b, c; unit cell volume; and α. As shown in Fig. 3(a), the compressibility of each direction is very anisotropic. Unexpectedly, the b axis has the largest compressibility with $\Delta b/b_0$ (intralayer) ~-9.5 (%/4 GPa), while other axes have $\Delta a/a_0$ (intralayer) $\approx\Delta c/c_0$ (interlayer) ~-4.7 (%/4 GPa). Such an anisotropic property can be seen in the typical AFD system associated with the AF-orbital ordering. In the case of $LaMnO_3$,[5] where AFD is formed in the ac plane, $\Delta a/a_0$ indicates a larger compressibility than $\Delta c/c_0\approx\Delta b/b_0$. In the case of K_2CuF_4,[16] where JTD is formed in the ab plane ($a=b$ tetragonal), $\Delta a/a_0=\Delta b/b_0$ indicates a larger compressibility than $\Delta c/c_0$. In such, the compounds with AFD as shown above, it is a significant feature that a large contraction takes place in the plane where the $3d$ orbitals are two-dimensionally ordered with the arrangement of the AFD of the elongated octahedron.

Figure 3(b) shows the pressure dependence of a unit cell volume. The observed compression property is continuous below P_c and shows a small change at P_c. This is completely different from the case of K_2CuF_4, where the volume changes markedly at 9.5 GPa.[16] The solid curve drawn through the volume data points in Fig. 3(b)

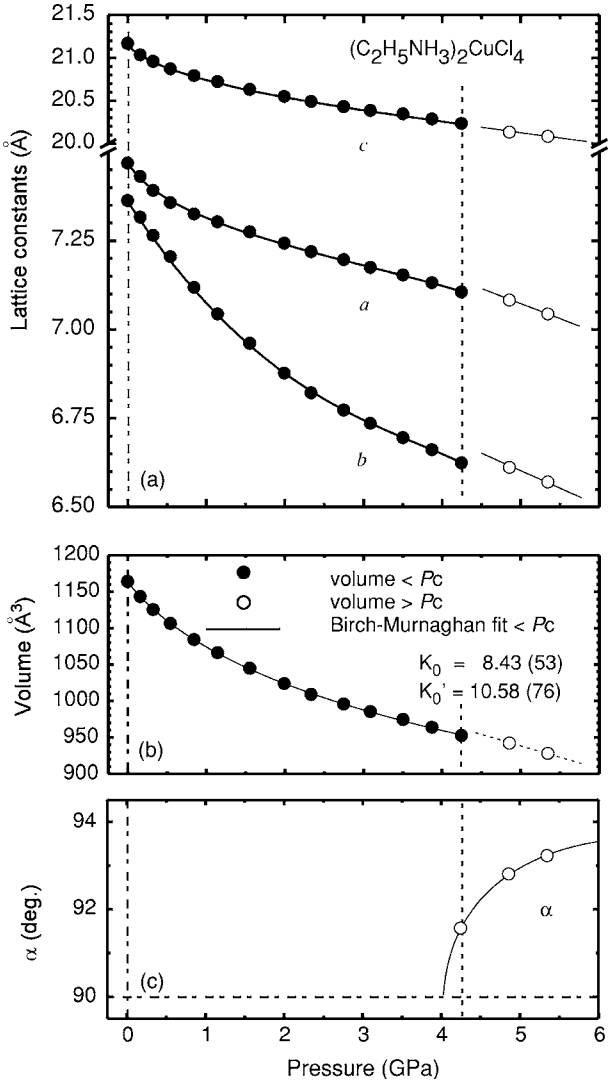

FIG. 3. Pressure dependence of lattice parameters. (a) Lattice constants a, b, and c. (b) Volume and Birch-Murnaghan fitting result (solid line). (c) α angle. Data obtained below P_c are shown by solid circles, while open circles denote data obtained above P_c. Solid lines drawn through the data in (a) and (c) are visual guides.

represents the result obtained by the least-squares-fit of the Birch-Murnaghan relation[17] with the bulk modulus K_0=8.43(53) GPa, K_0'=10.58(76) GPa. The K_0 of EA_2CuCl_4 is much smaller than those of the typical oxide $LaMnO_3$ (K_0=108 GPa)[5] and ionic crystal NaCl (K_0=23.77 GPa). We can expect that the structure of EA_2CuCl_4 changes markedly with a *small* pressure. Since the jump of the volume at P_c is very small and the evolution of α seems to be continuous, the phase transition is considered to be *weakly* of the first order.

We have also examined the pressure dependence of the crystal color (piezochromism) with a microscope at up to 5 GPa. The crystal color gradually changes from transparent yellow to red via orange. Figure 4 shows the photographs of the crystal of EA_2CuCl_4 in the DAC taken at 0.1 MPa and 5 GPa. Such an observed gradual color change corresponds to the large and gradual change of lattice

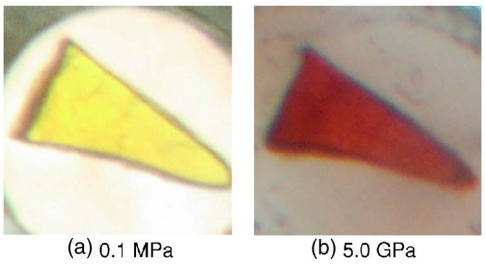

FIG. 4. (Color online) Piezochromizm of EA_2CuCl_1. Crystal color gradually changes from (a) yellow (0.1 MPa) to red (5.0 GPa) with pressure.

constants as shown in Fig. 3(a). What we observe is a complementary color of the absorption band of EA_2CuCl_4. The absorption energies corresponding to yellow and red are approximately 2.7 eV ($\triangleq$459.1 nm$\triangleq$21 776 cm^{-1}) and 2.3 eV ($\triangleq$539 nm$\triangleq$18 550 cm^{-1}).[18] Such an energy shift by 0.4 eV is consistent with the absorption measurements under pressure.[4] The energy gap characterized by the CT excitation from the ligand Cl 3p to the metal Cu 3d-hole site locates at approximately 3 eV (1 eV bandwidth) at AP and shifts to a lower energy by 0.4 eV under high pressure up to 4 GPa.[4] As seen from a band picture, the one-electron bandwidth of the 3d band increases due to the disappearance of the in-plane JTD.[4] Such a band broadening results in the redshift of the CT excitation.[4] The reddish transparency of the crystal indicates that the system is still insulative above P_c.

A yellow-to-light-green color change at a low temperature (thermochromism) is also reported.[1] Such a change in color must be due to the isotropic contraction of the $CuCl_6$ octahedron or further distortion by cooling.[19] Actually the CT excitation shows a blueshift by $\sim$0.1 eV,[20] which is consistent with the yellow-to-light-green color change.[21]

C. Suppression of JTD below P_c

To study the trend of such a reduction of JTD in EA_2CuCl_4 toward P_c, we performed the Rietveld analysis using powder diffraction patterns at pressures of 0.1 MPa and 0.68, 1.26, 1.99, 2.86, and 3.68 GPa. The program system RIETAN2000 has been used for the analysis.[22] We have assumed the space group D_{2h}^{15}-*Pbca* (No. 61) up to 4 GPa. By following the space group notation,[2] Cu is located on the 4a site, and Cl, C, and N on 8c sites. Cl1 is an apex chlorine of the $CuCl_6$ octahedron while Cl2 composes the two-dimensional plane of the $CuCl_6$ octahedron [see Figs. 1(a) and 1(b)]. For the present analysis, isotropic thermal parameters ($U_{eq}^2=B_{eq}/8\pi^2$ Å^2) are fixed to the values determined at atmospheric pressure using a single crystal;[1] U_{eq}^2(Cu)=0.0257, U_{eq}^2(Cl1)=0.0467, U_{eq}^2(Cl2)=0.0386, U_{eq}^2(N)=0.0418, and U_{eq}^2(C1)=U_{eq}^2(C2)=0.0684 Å^2. The observed and calculated diffraction patterns at 0.1 MPa are shown in Fig. 5. The discrepancy factor R_I of each analysis converges at approximately 10%. Using these refined parameters, we have calculated the pressure dependence of the three parameters Cu—Cl_{long}, Cu—Cl_{short}, and Cu—Cl_{apex} in the $CuCl_6$ octahedron as shown in

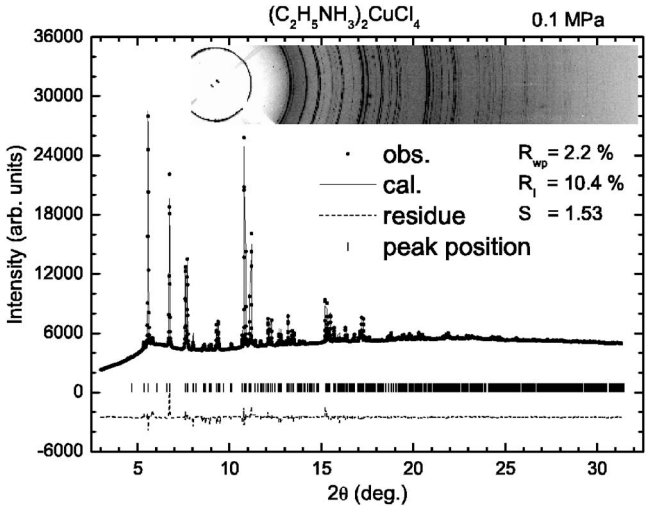

FIG. 5. Observed powder XRD pattern and Rietveld profile at 0.1 MPa. The inset shows the Debye-Scherrer rings recorded on an imaging plate.

Fig. 6, i.e., the Cu—Cl distance along the y, x, and z directions at the A site in Fig. 1(b), respectively. The structures of EA_2CuCl_4 in the ab plane at 0.1 MPa and 3.7 GPa are also shown in Fig. 6. The Cu—Cl_{long} distance gradually contracts, while the other two distances show no change with experimental resolution. The in-plane JTD is clearly suppressed by pressure application; however, a large distortion still remains just below P_c. The behavior of the reduction of JTD is consistent with the deactivation of the A mode.[4]

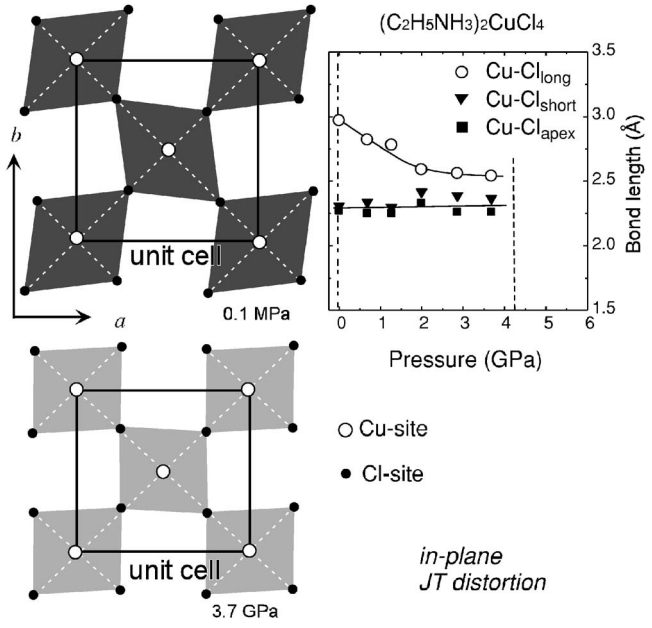

FIG. 6. Pressure dependences of three parameters Cu—Cl_{long}, Cu—Cl_{short}, and Cu—Cl_{apex} in $CuCl_6$ octahedron. The ab plane structures of EA_2CuCl_4 at 0.1 MPa and 3.7 GPa are also shown.

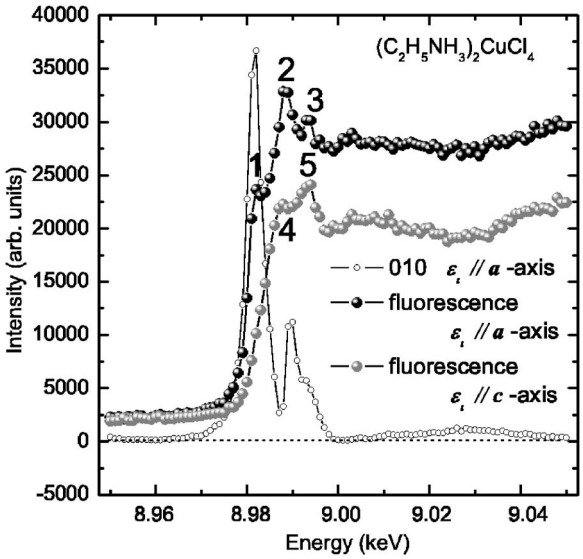

FIG. 7. Energy dependences of 010 *forbidden* reflection and fluorescence. 010 reflection with $\epsilon_i \| a$ and fluorescence with $\epsilon_i \| a$ and $\epsilon_i \| c$.

D. RXS study at ambient pressure

As mentioned in the Introduction, RXS intensity on the in-plane JT-distorted system is thought to well reflect the local distortion of the neighboring ligand ions.[8–12] To date, since JTD is suppressed, RXS intensity is expected to markedly change with a pressure. Prior to the RXS experiments conducted under a high pressure, we performed a precise RXS study at AP to understand the RXS characteristics of EA_2CuCl_4.

We have obtained the RXS intensities at the $0k0$ (k=odd) *forbidden*[23] spots just at the absorption edge of the Cu ion of EA_2CuCl_4, E=8.982 keV. Although we have also scanned at $h00$ and $00l$ (h,l=odd) forbidden spots, we cannot find any RXS intensities. Figure 7 shows the energy dependence of the 010 reflection with the polarization of incident x ray as the $\epsilon_i \| a$ axis and the fluorescence with the $\epsilon_i \| a$ axis and $\epsilon_i \| c$ axis. Several peaks as seen in the RXS energy spectra will be discussed later. It is quite obvious that the fluorescence profile strongly depends on the relationship between ϵ_i and crystal orientations (linear dichroism). The observed normalized RXS intensity of EA_2CuCl_4 ($I^{010}/I^{020} \sim 10^{-2}$) is obviously larger than that of manganite by $\sim$10.[26]

We have also measured the azimuthal angle dependence of the 010 RXS intensities at E=8.982 keV. Figure 8 shows the results of the measurements and the intensities that are normalized by the 020 fundamental reflection. The RXS intensities exhibit a characteristic oscillation with a twofold symmetry. The intensity reaches zero near ψ=0 and 180°, where it corresponds to the configuration in which the c axis is parallel to the polarization vector of the incident x ray ($\epsilon_i \| c$ axis). The same behavior can be seen at the other energy points in the energy spectrum of 010 RXS.

The results of RXS can be understood on the basis of a simple model proposed in Refs. 6 and 8, from which we can

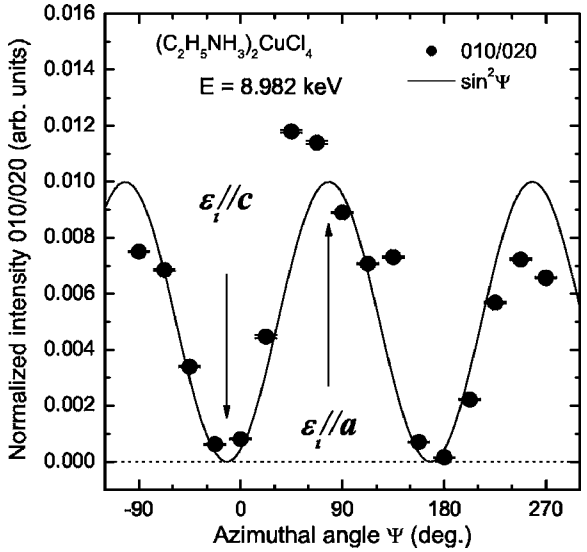

FIG. 8. Azimuthal angle dependence of RXS intensity of *forbidden* 010 reflection normalized by fundamental reflection 020 at $E=8.982$ keV. The solid curve denotes $\sin^2\psi$.

easily obtain the physical picture of the RXS intensities. A general formula will be shown in Appendix B. The RXS is described by a second-order process in which the incident photon is virtually absorbed due to a transition from the $1s$ state to the p state at Cu sites, followed by the emission of a photon due to the transition from the p state to the $1s$ state within the *dipole* approximation. Figure 1(b) shows the schematic drawing of one layer of EA_2CuCl_4. There are two sublattices, A and B sites, in the ab plane of EA_2CuCl_4 in Fig. 1(b). Here, we define the x, y, and z axes as shown in Fig. 1(b). We assume the scattering tensor at the $A(B)$ site $f^{A(B)}$ as

$$f^{\mathrm{A(B)}}=\begin{pmatrix} M_{xx}^{\mathrm{A(B)}} & 0 & 0(1) \\ 0 & M_{yy}^{\mathrm{A(B)}} & 0(2) \\ 0 & 0 & M_{zz}^{\mathrm{A(B)}} \end{pmatrix}. \tag{1}$$

The RXS amplitude $M_{\alpha\beta}$ $(\alpha,\beta=x,y,z)$ is described as

$$M_{\alpha\beta}(\omega)=\sum_j \frac{\langle 1s|r_\alpha|p_j\rangle\langle p_j|r_\beta|1s\rangle}{\omega-(\omega_j-\omega_{1s})+i\Gamma}, \tag{2}$$

where ω is the energy of the incident and emitted photons, and Γ is the lifetime broadening width of the $1s$ core hole, ~ 2 eV. The energies ω_{1s} and ω_j correspond to the core state $|1s\rangle$ and the excited p state $|p_j\rangle$, respectively. The off-diagonal elements of the scattering tensor are negligible at present. Since all the Cu sites are crystallographically equivalent in EA_2CuCl_4, the amplitude at A and B sites are related as $M_{xx}^A=M_{yy}^B$, $M_{yy}^A=M_{xx}^B$, and $M_{zz}^A=M_{zz}^B$. For the present experimental setup, the RXS intensities are given by

$$I^{0k0}=I_{\sigma\sigma'}^{0k0}+I_{\sigma\pi'}^{0k0}\propto|M_{xx}^{\mathrm{A}}-M_{xx}^{\mathrm{B}}|^2\cos^2\theta\sin^2\psi, \tag{3}$$

where $I_{\sigma\sigma'}^{0k0}=0$, and θ and ψ are the Bragg and azimuthal angles, respectively. Equation (3) shows that the RXS intensities reflect the difference in the DOS between the p_x and p_y symmetries. The calculation shows that only the $0k0$ (k=odd) reflections are observable in EA_2CuCl_4, which agrees well with the experimental results. This is due to the assumption that the scattering tensor is expressed as Eq. (1), where the octahedron has no tilt, that is, the ab plane of EA_2CuCl_4 is regarded as a *pseudo* mirror plane. See Appendix B for a general approach to RXS. It also well represents the twofold feature of the azimuthal angle dependence of the RXS intensities as shown in Fig. 8 by the solid line.

On the other hand, the fine structure of the fluorescence in the near-edge region can be understood by an analogy with La_2CuO_4,[24] where core-hole screening is taken into account. As is well known, fluorescence intensity yields essentially the same results as more conventional *transmission* experiments.[25] By comparing with the assignments performed on La_2CuO_4,[24] which has the same crystal structure as that of EA_2CuCl_4, the five peaks labeled 1 to 5 in Fig. 7 can be assigned as $|\underline{c}3d^{10}\underline{L}4p_y\rangle$, $|\underline{c}3d^9 4p_y\rangle + |\underline{c}3d^{10}\underline{L}4p_x\rangle$, $|\underline{c}3d^9 4p_x\rangle$, $|\underline{c}3d^{10}\underline{L}4p_z\rangle$, and $|\underline{c}3d^9 4p_z\rangle$, respectively, where $\underline{L}$ is a ligand hole and $\underline{c}$ is a core hole. All peaks are assigned to the A site; such peak assignments will be used hereafter unless otherwise mentioned. The $3d^{10}\underline{L}$ configurations have an effect of core-hole screening (well screened), while the $3d^9$ configurations have an effect of poor screening. It is expected that the weight of the $3d^{10}\underline{L}$ configurations will decrease when the degree of ionicity of the ligand increases. In the case of EA_2CuCl_4, the intensity of $|\underline{c}3d^{10}\underline{L}4p\rangle$ is smaller than $|\underline{c}3d^9 4p\rangle$ as shown in Fig. 7. While, in the case of La_2CuO_4, the intensity of $|\underline{c}3d^{10}\underline{L}4p\rangle$ is larger than that of $|\underline{c}3d^9 4p\rangle$.[24] These results indicate that the ionicity in EA_2CuCl_4 is stronger than that in La_2CuO_4.

Since the DOS of the $4p_x^A$ $(4p_y^B)$ symmetry is thought to be nearly equal to that of the $4p_z^{A(B)}$ symmetry because of the $d_{x^2-z^2}$ hole-orbital occupation, we can derive the energy dependence of each component of the absorption spectra with the $\epsilon_i\|ab$ plane, that is $\mu_{xx}(E)$ and $\mu_{yy}(E)$ as shown in Fig. 9(a). $\mu_{xx}(E)$ and $\mu_{yy}(E)$ are derivable as follows. First, we fit the edge jump of the two fluorescence spectrum in Fig. 7 by comparing the calculated absorption spectrum of EA_2CuCl_4. Then, some corrections are made for a self-absorption effect of the incident and the scattered x ray. At this stage, we have the absorption spectrum $1/2[\mu_{xx}(E)+\mu_{yy}(E)]$ from the fluorescence with the $\epsilon_i\|ab$ plane and μ_{zz} from the fluorescence with the $\epsilon_i\|c$ axis. Although, the DOS of the $4p_x^A$ $(4p_y^B)$ symmetry is thought to be nearly equal to the $4p_z^{A(B)}$ symmetry, the $\mu_{zz}(E)$ is regarded as $\mu_{zz}(E)\approx\mu_{xx}(E)$. Therefore, $\mu_{yy}(E)$ is finally derived as $\mu_{yy}(E)\approx[\mu_{xx}(E)+\mu_{yy}(E)]-[\mu_{zz}(E)]$.

Here, note that the difference between $\mu_{xx}(E)$ and $\mu_{yy}(E)$ can provide the 010 RXS spectra as seen in Fig. 7. So, we first assume the following equation and then compare with the RXS spectra:

$$I_{cal.}(E)\propto|\mu_{xx}(E)-\mu_{yy}(E)|^2\bar{\mu}. \tag{4}$$

Here, $\bar{\mu}$ is the absorption coefficient of the present sample EA_2CuCl_4, which is equal to $\mu_{xx}(E)+\mu_{yy}(E)$ with the $\epsilon_i\|a$

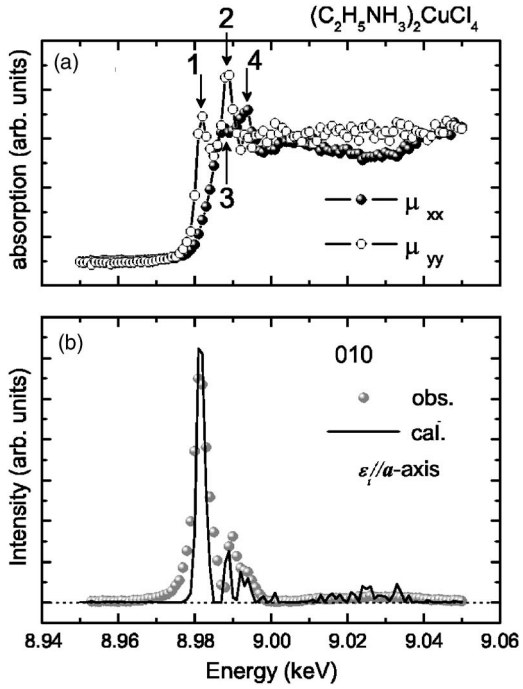

FIG. 9. (a) Two derived components of fluorescence (=absorption) spectra with $\epsilon_i \| ab$ plane, μ_{xx} and μ_{yy}. (b) Comparison of the spectrum calculated from Eq. (4) with the observed spectrum.

axis incident x ray. Figure 9(b) shows a comparison between the calculated (solid line) and observed (solid circles) spectra. It is clear that the calculated spectrum reproduces the observed 010 RXS spectrum very well. The sharp peak structure between $E=8.98$ and 9.00 keV and the broad peak structure between $E=9.00$ and 9.05 keV are almost perfectly reproduced by Eq. (4). The present calculation results obtained using Eq. (4) led us to consider that the imaginary part of the scattering amplitude $|M^A_{xx}-M^B_{xx}|$ in Eq. (3) is dominant over the present RXS spectra of EA_2CuCl_4. The difference between the observed and calculated profiles seen at the base of the sharp peaks at $E=8.982$ keV may be due to a contribution of the real part of the scattering amplitude. Generally, the absorption coefficient $\mu(E)$ is proportional to the imaginary part of the anomalous scattering factor $f''(E)$ and is directly related to the DOS of the p symmetry. That is to say, the present RXS spectrum well reflects the difference in DOS between the p_x and p_y symmetries of the Cu ion. At this stage, we can clearly reassign the four peaks labeled 1 to 4 in Fig. 9(a) as $|\underline{c}3d^{10}\underline{L}4p_y\rangle$, $|\underline{c}3d^9 4p_y\rangle$, $|\underline{c}3d^{10}\underline{L}4p_x\rangle$, and $|\underline{c}3d^9 4p_x\rangle$, respectively. It is clear that the strongest peak at $E=8.982$ keV is dominated by the $|\underline{c}3d^{10}\underline{L}4p_y\rangle$ intermediate state. By an analogy with $LaMnO_3$,[8–11] it is thought that the difference in the DOS of the EA_2CuCl_4 system mainly comes from the JTD of the $CuCl_6$ octahedron, which is termed JT mechanism hereafter. The JT mechanism contains two types of mechanisms that provide the difference in the DOS. One is the hybridization between the Cu $4p$ and the Cl $2p$ orbitals and the other is the repulsive potential of the negatively charged Cl ions neighboring the Cu site. However the present experimental results cannot select either. If the on-site $3d$-$4p$ Coulomb interaction,[26,27] which is termed Coulomb mechanism hereafter, is dominant in this system, the energy scheme will be reversed between μ_{xx} and μ_{yy} in Fig. 9(a).

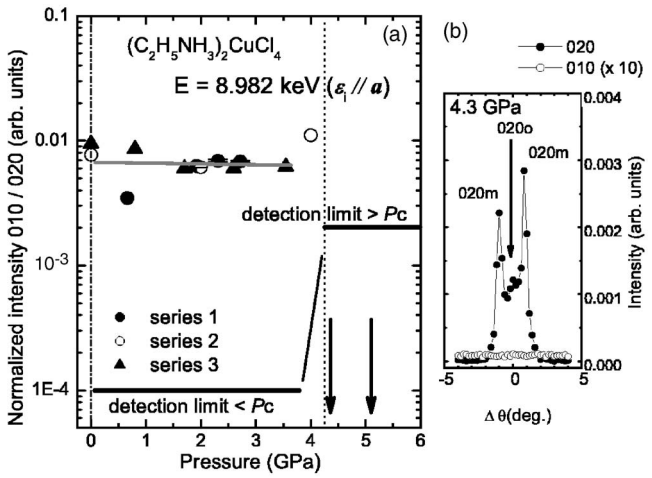

FIG. 10. (a) Pressure dependence of the normalized RXS intensity I^{010}/I^{020} observed at $E=8.982$ keV. (b) 020 peak profile observed just above the transition pressure $P=4.3$ GPa. Two-phase coexistence (020_o and twin 020_m) is still seen. The corresponding 010 RXS signal was not observed down to the detection limit of $\sim 2\times 10^{-3}$ of the 020 intensity. The 010 profile is magnified by a factor of 10.

E. RXS study under high pressure

Up to this point, we have investigated the effects of hydrostatic pressure on the lattice and structure of EA_2CuCl_4 and the precise RXS characteristics of EA_2CuCl_4 at AP. The suppression of the JT effects, which is predicted by the Raman scattering measurement[4] is ascertained by the structural analyses below the transition pressure P_c as shown in Secs. III A–III C. The observed 010 RXS spectrum well reflects the difference in DOS between the p_x and p_y symmetries of the Cu ion, which is mainly dominated not by the Coulomb mechanism but by the JT mechanism. If so, the RXS intensity changes as the pressure increases, i.e, with the suppression of the JT effects. Next, we performed the RXS study under a high pressure.

We particularly focused on the strongest peak at $E=8.982$ keV, which is dominated by the $|\underline{c}3d^{10}\underline{L}4p_y\rangle$ intermediate state. Figure 10(a) shows the pressure dependence of the normalized RXS intensity I^{010}/I^{020}. As the pressure increases, unexpectedly, the 010 RXS intensity shows no marked change below P_c, while the intensity becomes zero above P_c down to the detection limit $\sim 2\times 10^{-3}$ of the 020 intensity. Incidentally, the existence of the phase transition at P_c guarantees that no irradiation damage is induced, as discussed in Appendix A.

Figure 10(b) shows the 020 peak profile observed just above the transition pressure, $P=4.3$ GPa. We investigated RXS intensity around the 010 and 100 spots with sufficient statistics just above P_c ($P=4.3$ GPa), where the orthorhombic-low-pressure phase and the monoclinic-

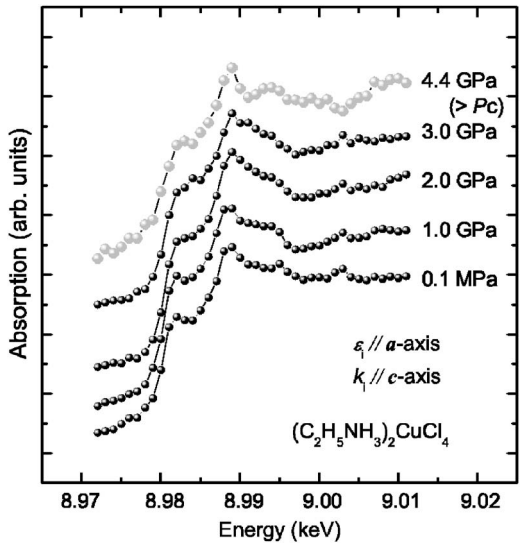

FIG. 11. X-ray absorption spectra of EA_2CuCl_4 measured at 0.1 MPa, 1.0 GPa, 2.0 GPa, 3 GPa, and 4.4 GPa ($>P_c$).

high-pressure phase coexist, and far above P_c ($P=5.1$ GPa) [see two arrows in Fig. 10(a)]. However, we could not determine any RXS intensity down to the detection limit of $\sim 2\times 10^{-3}$ of 020 intensity [see solid line in Fig. 10(a)]. The peak width broadening above P_c results in the change of the detection limit at the phase boundary and lowers the efficiency of the detection of the 010 peak.

To confirm the invariability of RXS intensity below P_c and the sudden suppression of this intensity above P_c, we measured the x-ray absorption spectrum of EA_2CuCl_4, which directly reflects DOS (p_x and p_y symmetries), at 0.1 MPa, 1.0 GPa, 2.0 GPa, 3.0 GPa, and 4.4 GPa ($>P_c$) as shown in Fig. 11. A slight blueshift of the peaks labeled 1 and 2 in Fig. 7 and a redshift of the peak labeled 3 in Fig. 7 can be seen. The weak blueshift and redshift of the absorption spectrum are due to the suppression of the JTD of the $CuCl_6$ octahedron. However, no significant change in the overall structure near the absorption edge has been observed. The shoulder, which originates from $|\underline{c}3d^{10}\underline{L}4p_y\rangle$ and gives the main RXS intensity at $E=8.982$ keV, can still be clearly seen at 3 GPa. This is consistent with the behavior of the RXS intensity under a high pressure. These results indicate that the DOS of the p_x and p_y symmetries of EA_2CuCl_4 does not significantly change with pressure application below P_c.

From the first-principle calculation for $LaMnO_3$ and $KCuF_3$, the RXS intensities increase as the DOS of the p_x and p_y symmetries polarizes.[8–12] The calculation also indicates that the polarization depends on the q value,[28] which is directly related to the degree of JTD. In the case of EA_2CuCl_4, the q value ($q\sim 0.7$ Å) is much larger than those of $LaMnO_3$ ($q\sim 0.27$ Å)[29] and $KCuF_3$ ($q\sim 0.36$ Å).[12] It is expected that the polarization of the DOS of the p_x and p_y symmetries of EA_2CuCl_4 saturates and hardly shows further changes, so that the DOS shows a slight change as shown in Fig. 11 even as the Cu—Cl_{long} distance markedly decreases as seen in Fig. 6. After the large JTD suppression, the RXS intensity will start to be sensitive to the suppression of JTD.

The RXS behavior near P_c is discussed. First, we compare the high-pressure phase of EA_2CuCl_4 with the AP phase of MA_2CuCl_4, both of which have the same space group $P2_1/a$. Although it is not shown in this paper, MA_2CuCl_4 has the same types of JT-distorted $CuCl_6$ octahedron and provides a large RXS intensity (the same order as that in the present EA_2CuCl_4 case) at AP at the 100 spot, which is equivalent to the 010 spot with the *Pbca* setting as observed in EA_2CuCl_4 at AP. On the other hand, the RXS intensity of EA_2CuCl_4 above P_c becomes zero. Namely, the local structure around the Cu site of the high-pressure phase of EA_2CuCl_4 is considerably different from that of the AP phase of MA_2CuCl_4. In MA_2CuCl_4, the intensities of the Raman-active modes from JTD continuously decrease with increasing pressure below 3 GPa similar to the case of EA_2CuCl_4. However, these intensities suddenly recover above ~ 3.6 GPa accompanied by shifts in their mode frequencies toward the low-energy side.[4] Contrary to EA_2CuCl_4, this indicates an onset of another type of structural transition and that the high-pressure non-JT-distorted phase is unstable in MA_2CuCl_4. Present results that the RXS intensity becomes zero beyond the detection limit, indicate that the scattering amplitude $|M_{xx}^A - M_{xx}^B|$ in Eq. (3) significantly decreases or reaches zero. The decrease in amplitude means that the in-plane Cu—Cl distances, which are related to the polarization of DOS on the Cu site, are equal to each other. From these results, we can speculate that the DOSs of the p_x and p_y symmetries become nearly equal to each other above P_c. However, the XAS spectrum taken at 4.4 GPa shows no significant change. The relationship between the structure and the XAS spectrum above P_c remains open to be solved.

The present experimental results and the reported Raman scattering results[4] provide at least three possible conditions for the formation of the structure of EA_2CuCl_4 above P_c. The first one is that JTD is completely suppressed. The second one is that La_2CuO_4-like JTD is induced, where Cu—O_{long} stands ferrodistortively perpendicular to the *ab* plane ($d_{x^2-y^2}$ hole-orbital ordering). The former case is the same as the intermediate Mott-Hubbard insulating state of the $LaMnO_3$ under pressure.[5] In each case, the nearest-neighbor $CuCl_6$ octahedron tilts alternately along the *b* direction to conserve all Cu—Cl distances equal in the $CuCl_4$ plane under the condition $a>b$ under a high pressure. The two significantly different lengths between *a* and *b* will produce a zigzag arrangement of octahedra in the *ab* plane as shown in Fig. 12. The tilting behavior will propagate to the nearest layer via the $C_2H_5NH_3^+$ molecular section (see Fig. 1) and finally makes the system monoclinic as experimentally determined. This is the same as that of the AP phase of MA_2CuCl_4. The tilting behavior also provides the antiphase domains as clarified by the twin peaks above P_c in Fig. 2. The third possibility, high-pressure K_2CuF_4-type JTD where Cu F_{long} lies ferrodistortively in the *ab* plane[16] ($d_{x^2-z^2(y^2-z^2)}$ hole-orbital ordering), is ruled out by the determined unit cell as presented in Sec. III A.

IV. CONCLUSIONS

The effects of hydrostatic pressure on the structure and the corresponding RXS spectra have been investigated for

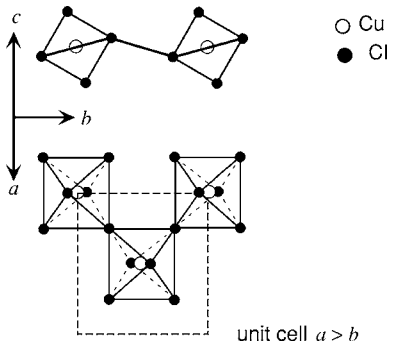

FIG. 12. Schematic drawing of the zigzag arrangement of $CuCl_6$ octahedra in the *ab* plane. The marked difference between the lattice constants *a* and *b* results in the structure.

the AF-hole-orbital-ordered system EA_2CuCl_4.

The structural phase transition at $P_c \sim 4$ GPa, which is suggested by the Raman scattering measurement,[4] is confirmed by observing a peak splitting resulting from an orthorhombic-to-monoclinic phase transition. The possible space group of the high-pressure phase is $P2_1/a$, which is the same as that of MA_2CuCl_4. The suppression of JTD below P_c[4] is also ascertained by structural analyses. Piezochromism is also observed in connection with the structural change below and above P_c. The red-colored transparency of the crystal indicates that the system is still insulative above P_c.

The observed RXS and fluorescence spectra at AP were precisely analyzed. We experimentally confirmed that the RXS comes from the polarization of the DOS of the p_x and p_y symmetries, which is mainly dominated not by the Coulomb mechanism but by the JT mechanism. Such a mechanism of the RXS was already given by the first-principles calculation.[8–12] The calculation shows that RXS intensity increases as the JTD evolves, while our RXS study under a high pressure shows no striking change with the suppression of JTD by pressure application. The present invariable behavior of RXS intensity is thought to be a particular characteristic of largely distorted JT systems such as EA_2CuCl_4, i.e., the modification of DOS, which provides RXS intensity, already saturates in such markedly distorted JT systems. In such systems, RXS intensity will not be sensitive at the beginning of the suppression of JTD.

On the other hand, the RXS intensity becomes zero above P_c. The results indicate that the local environment of the Cu^{2+} ion markedly changes. In the present study, we proposed two possible electronic states of EA_2CuCl_4 above P_c. One is, completely suppressed JTD associated with hole-orbital-ordering melt, the other is the La_2CuO_4-like JTD associated with F-orbital-ordering induction. The former case is the same as the intermediate Mott-Hubbard insulating state of $LaMnO_3$ under pressure.[5]

Finally, the relationship between the structure and XAS spectrum of EA_2CuCl_4 above P_c is yet to be determined.

As presented in the introduction, the ordering pattern of the hole orbital determines the magnetic interaction between Cu sites. Therefore, it is interesting what type of magnetic interaction is generated and what type of magnetic order takes place above P_c in EA_2CuCl_4. Further experimental investigations focusing on magnetic properties such as neutron scattering and magnetic susceptibility measurements are required to solve these questions.

ACKNOWLEDGMENTS

We would like to thank Dr. M. Usuda, Dr. J. Igarashi, and Dr. T. Yoshinari for stimulating discussions, as well as Dr. Y. Wakabayashi and Dr. H. Sawa (Photon Factory) for technical support. We also give special thanks to Mr. T. Mori for total support. This work was supported in part by a Grant-In-Aid for Scientific Research from MEXT (Proposal No. 14740221). The synchrotron radiation experiments were performed at SPring-8 with the approval of the Japan Synchrotron Radiation Research Institute (JASRI) (Proposal No. 2001B0322-ND-np, No. 2002B0278-ND2-np), and at the Photon Factory with the approval of the Advisory Committee (Proposal No. 2001S2002).

APPENDIX A: IRRADIATION EFFECTS

At the beginning of the RXS experiments, we faced the problem of *irradiation effects*. A large number of photons are absorbed just above the Cu *K*-absorption edge and samples are seriously damaged. This can be clearly seen by monitoring fundamental Bragg intensities such as that for 020. Under x-ray irradiation, Bragg intensity decreases by a factor of 10^{-1} ($\sim$3 min) with the incident 10^{11} (photons/mm^2 s) at BL02B1/SPring-8. The crystal immediately becomes black after the irradiation. So, we have performed all RXS experiments very carefully by reducing the number of photons by a factor of 10^{-3} with an aluminum absorber for elongation of the lifetime of the crystal. Since the damaged crystal shows no clear phase transition at P_c, we can easily know how much the crystal is damaged by observing the phase transition. For the present experiment, the phase transition is observed at P_c as shown in Fig. 10(b). Such irradiation effects are generally measured for the alkylammonium tetrachloro-transition metal $(C_nH_{2n+1}NH_3)_2MCl_4$ ($n=1,2,3$; $M=$Mn, Cu, Cd).[30–32]

APPENDIX B: ANOTHER APPROACH TO THE STRUCTURAL FACTOR TENSOR OF RXS

We present the general formula of the structural factor tensor of RXS of EA_2CuCl_4 for the indices 100, 010, and 001. We define the principal axis of the unit cell as the axis of the coordinates of the scattering amplitude [see Fig. 1(b)] and introduce the following scattering tensor at a Cu site (4a site of space group D_{2h}^{15}-*Pbca*):

$$f_{\mathrm{Cu}} = \begin{pmatrix} M_{aa} & M_{ab} & M_{ac} \\ M_{ab} & M_{bb} & M_{bc} \\ M_{ac} & M_{bc} & M_{cc} \end{pmatrix} \tag{B1}$$

By summing up the four symmetrically operated tensors of the four equivalent Cu sites in a unit cell, we can obtain the structural factor tensor of the 100, 010, and 001 reflections, as follows:

$$F^{100} = 4\begin{pmatrix} 0 & 0 & M_{ac} \\ 0 & 0 & 0 \\ M_{ac} & 0 & 0 \end{pmatrix}, \quad \text{(B2)}$$

$$F^{010} = 4\begin{pmatrix} 0 & M_{ab} & 0 \\ M_{ab} & 0 & 0 \\ 0 & 0 & 0 \end{pmatrix}, \quad \text{(B3)}$$

$$F^{001} = 4\begin{pmatrix} 0 & 0 & 0 \\ 0 & 0 & M_{bc} \\ 0 & M_{bc} & 0 \end{pmatrix}. \quad \text{(B4)}$$

Since the 100 and 001 reflections have not been observed in EA_2CuCl_4, the scattering amplitudes M_{ac} and M_{bc} are nearly equal to zero. This result indicates that the *ab* plane of EA_2CuCl_4 is regarded as a pseudomirror plane. That is, the tilting angle of the $CuCl_6$ octahedron is very small.

*Corresponding author. Electronic address: ohwada@spring8.or.jp; Also at CREST, Japan Science and Technology Agency (JST), Kawaguchi 332-0012, Japan.

†Also at Department of Physics, Tohoku University, Sendai 980-8578, Japan.

[1] J. P. Steadmen and R. D. Willett, Inorg. Chim. Acta **4**, 367 (1970).

[2] *International Tables for Crystallography, Vol. A*, edited by Theo Hahn (Reidel Publishing Company, 1983).

[3] Y. Itoh and J. Akimistu, J. Phys. Soc. Jpn. **40**, 1333 (1976).

[4] Y. Moritomo and Y. Tokura, J. Chem. Phys. **101**(3), 1763 (1994).

[5] I. Loa, P. Adler, A. Grzechnik, K. Syassen, U. Schwarz, M. Hanfland, G. Kh. Rozenberg, P. Gorodetsky, and M. P. Pasternak, Phys. Rev. Lett. **87**, 125501 (2001).

[6] Y. Murakami, J. P. Hill, D. Gibbs, M. Blume, I. Koyama, M. Tanaka, H. Kawata, T. Arima, Y. Tokura, K. Hirota, and Y. Endoh, Phys. Rev. Lett. **81**, 582 (1998).

[7] L. Paolasini, R. Caciuffo, A. Sollier, P. Ghigna, and M. Altarelli, Phys. Rev. Lett. **88**, 106403 (2002).

[8] M. Takahashi, J. Igarashi, and P. Fulde, J. Phys. Soc. Jpn. **68**, 2530 (1999).

[9] M. Benfatto, Y. Joly, and C. R. Natoli, Phys. Rev. Lett. **83**, 636 (1999).

[10] I. S. Elfimov, V. I. Anisimov, and G. A. Sawatzky, Phys. Rev. Lett. **82**, 4264 (1999).

[11] P. Benedetti, J. van den Brink, E. Pavarini, A. Vigliante, and P. Wochner, Phys. Rev. B **63**, 060408(R) (2001).

[12] M. Takahashi, M. Usuda, and J. I. Igarashi, Phys. Rev. B **67**, 064425 (2003).

[13] H. K. Mao, P. M. Bell, J. W. Shaner, and D. J. SteinBerg, J. Appl. Phys. **49**, 3276 (1978).

[14] Pressure was calibrated from a lattice constant of NaCl enclosed with the specimen in the DAC. A numerical formula is reported in C. S. Menoni and I. L. Spain, High Temp. - High Press. **16**, 119 (1984).

[15] I. Pabst, H. Fuess, and J. W. Bats, Acta Crystallogr., Sect. C: Cryst. Struct. Commun. **C43**, 413 (1987).

[16] M. Ishizuka, M. Terai, M. Hidaka, S. Endo, I. Yamada, and O. Shimomura, Phys. Rev. B **57**, 64 (1998).

[17] J. R. Macdonald and D. R. Powell, J. Res. Natl. Bur. Stand., **75A**, 441 (1971). The Birch-Murnaghan relation is $P = 3/2K_0[(V_0/V)^{7/3} - (V_0/V)^{5/3}]\{1 - 3/4(4 - K_0')[(V_0/V)^{2/3} - 1]\}$, where $K_0' = dK_0/dP$.

[18] 1 eV ≙ 8065.54 cm^{-1} ≙ 1239.8 nm; "≙" is used to express "equivalent to" or "corresponding to" in this paper.

[19] R. Valiente and F. Rodriguez, Phys. Rev. B **60**, 9423 (1999).

[20] V. Kapustianik, Yu. Korchak, I. Polovinko, R. Tchukvinskyi, Z. Czapla, and S. Dacko, Phys. Status Solidi B **207**, 95 (1998).

[21] The color of the crystal is reported in Ref. 1 as light green. The color is probably *yellowish* green, which is a complementary color of violet (the absorption band; 400 nm ~435 nm) and is consistent with the blue shift of CT excitation (see Ref. 20).

[22] F. Izumi and T. Ikeda, Mater. Sci. Forum **321–324**, 198 (2000).

[23] As for the *normal* X-ray diffraction, the general reflection conditions of the space group *Pbca* are 0*kl*, *h*0*l*, *hk*0, *h*00, 0*k*0, and 00*l* (h,k,l=even). The reflections satisfying the h,k,l=odd conditions are *forbidden*. See. Ref. 2, No. 61.

[24] H. Tolentino, M. Medarde, A. Fontaine, F. Baudelet, E. Dartyge, D. Guay, and G. Tourillon, Phys. Rev. B **45**, 8091 (1992).

[25] J. Jaklevic, J. A. Kirby, M. P. Klein, A. S. Robertson, G. S. Brown, and P. Eisenberger, Solid State Commun. **23**, 679 (1977).

[26] S. Ishihara and S. Maekawa, Phys. Rev. Lett. **80**, 3799 (1998).

[27] S. Ishihara and S. Maekawa, Phys. Rev. B **58**, 13442 (1998).

[28] q is defined as , where M-L_{long} and M-L_{short} denote the long and short M-L distances in the JT-distorted ML_4 plane (M:3*d* transitional metal, L:ligand, respectively).

[29] J. Rodriguez-Carvajal, M. Hennion, F. Moussa, A. H. Moudden, L. Pinsard, and A. Revcolevschi, Phys. Rev. B **57**, R3189 (1998).

[30] T. Yoshinari, T. Ebihara, I. Kotani, Y. Sato, A. Suzuki, Y. Seino, K. Masuda, T. Yano, K. Yumura, K. Wako, T. Matsuyama, and K. Aoyagi, J. Phys. Soc. Jpn. **59**, 2998 (1990).

[31] T. Yoshinari, Phase Transitions **36**, 89 (1991).

[32] T. Yoshinari, S. Shimanuki, T. Matsuyama, H. Yamaoka, and K. Aoyagi, Nucl. Instrum. Methods Phys. Res. B **91**, 230 (1994).